Coordinate control of gene expression noise and interchromosomal interactions in a MAPK pathway

Emma McCullagh[1], **Anupama Seshan**[1,2], **Hana El-Samad**[1,3], and **Hiten D. Madhani**[1,3]

[1]Department of Biochemistry and Biophysics, University of California, San Francisco, 600 16th St. San Francisco, CA 94158

Abstract

In the *Saccharomyces cerevisiae* pheromone-response pathway, the transcription factor Ste12 is inhibited by two MAP kinase-responsive regulators, Dig1 and Dig2. These two related proteins bind to distinct regions of Ste12 but are redundant in their inhibition of Ste12-dependent gene expression. Here we describe three unexpected functions for Dig1 that are non-redundant with those of Dig2. First, the removal of Dig1 results in a specific increase in intrinsic and extrinsic noise in the transcriptional outputs of the mating pathway. Second, in *dig1* cells, Ste12 relocalizes from the nucleoplasmic distribution seen in wild-type cells into discrete subnuclear foci. Third, genome-wide iChIP studies revealed that Ste12-dependent genes display increased interchromosomal interactions in *dig1* cells. These findings suggest that the regulation of gene expression through long-range gene interactions, a widely-observed phenomenon, comes at the cost of increased noise. Consequently, cells may have evolved mechanisms to suppress noise by controlling these interactions.

Cells respond to environmental fluctuations by transducing signals to networks of DNA-binding proteins. Numerous transcriptional regulators, including p53[1], E2Fs[2] and Smads[3,4], are subject to overlapping inhibitory mechanisms, yet the logic underlying these potential circuit redundancies remains poorly understood. A well-defined example of such regulatory architecture occurs in the *S. cerevisiae* mating pathway in which the transcription factor Ste12 is inhibited by two MAP kinase-responsive regulators, Dig1 and Dig2. These related proteins are redundant in their suppression of Ste12 activity since the removal from cells of both proteins is required to de-repress pathway activity[5,6]. Despite this redundancy Dig1 and Dig2 bind to distinct regions of Ste12; Dig1 to the activation domain and Dig2 to the DNA-binding domain[7,8].

[3]Correspondence should be addressed to H.D.M. (hitenmadhani@gmail.com) and H.E-S. (Hana.El-Samad@ucsf.edu) .
[2]Present address: Department of Biology, Emmanuel College, 400 The Fenway, Boston, MA 02115

Author Contributions

E.M. constructed all strains and performed and analyzed all experiments except for the FACS-based mating assay. A.S. constructed strains for and performed the FACS-based mating assay. H.E-S. and E.M. wrote custom MATLAB software and conducted data analyses for the FACS assays. E.M., H. E-S. and H.D.M. wrote the manuscript.

Competing Financial Interests

The authors declare no competing financial interests.

Methods

Methods and associated references are available in the online version of the paper at http://www.nature.com/naturecellbiology

Ste12 lies at the terminus of a signal transduction pathway that is initiated by the binding of extracellular pheromones to a G-protein coupled receptor. This ligand-sensing event triggers the activation of a MAP kinase (MAPK) cascade, which initiates a cytoplasmic response and transmits the mating signal to the nucleus to activate the transcription factor Ste12 (Fig. 1a). Ste12 regulates the expression of a network of genes whose products are required for the process of mating. Unstimulated cells display a basal level of signalling that increases upon stimulation with pheromone. This system has been utilized recently as a model to measure variability, or noise, in a signal transduction cascade and to ascertain whether such noise is controlled[9,10]. Interestingly, it was found that removal of either of the MAPKs, Fus3 or Kss1, did not affect total output variability, suggesting that this natural system may have evolved overlapping mechanisms that buffer against noise[9]. Since the regulation of gene expression noise has been suggested to be important for appropriate input-output responses[11-13], we reasoned that the investigation of noise in the output of the mating pathway might reveal mechanisms that underlie the redundant regulatory architecture controlling Ste12 activity.

RESULTS

Noise in Ste12-dependent gene expression outputs is limited by Dig1

We constructed two Ste12-dependent reporter genes, *pAGA1-YFP* and *pFUS1-YFP*. Their output distributions in wild-type and *dig1* cells overlapped less than 5% with the background autofluorescence of yeast (Supplementary Information, Fig. S1). The mean output of *dig1* strains increased 1.4-fold over wild-type, while mean fluorescence levels in *dig2* did not change measurably (Fig. 1b), confirming that Dig1 and Dig2 appear redundant in their inhibition of average Ste12-dependent transcription[5,6] when assayed in this manner. As expected, deleting *DIG1* and *DIG2* resulted in a 19-fold and 9-fold increase in mean expression for *pAGA1-YFP* and *pFUS1-YFP*, respectively (Fig. 1b). The mean output of a Ste12-independent reporter, *pPMP1-GFP*, was unaffected by deletion of *DIG1* or *DIG2* (Fig. 1b).

In contrast, examination of the single-cell output distributions of the Ste12-dependent reporters revealed a non-redundant role for Dig1 that is distinct from Dig2. Deletion of *DIG1*, but not *DIG2*, significantly increased the variability as measured quantitatively by the coefficient of variation or CV (Fig. 1c), and qualitatively by the spread of the *pAGA1-YFP* and *pFUS1-YFP* distributions (Fig. 1d). The CVs of the *pFUS1-YFP dig1* and *pAGA1-YFP dig1* output distributions were 29.6% ($P = 0.0003$) and 12.5% ($P = 0.0014$) higher, respectively, than those of wild-type and *dig2* (Fig. 1c,d). Cell sorting experiments indicated that a cell population isolated from the middle of the *dig1* output distribution could regenerate the entire distribution within 1-2 cell cycles (Fig. 2). Thus, while the steady-state fraction of cells experiencing the high-expression state at any given time point in the *dig1* mutant is modest, the entire population of *dig1* cells is likely to dynamically experience inappropriately high-expression states over time. The larger CV of *dig1* output distributions was unexpected, and all the more significant, because the slight increase in mean output in *dig1* cells might be predicted to generate a decrease, rather than an increase, in noise[14]. Furthermore, the increase in noise in *dig1* cell populations was

independent of forward scatter and side scatter, flow cytometric surrogate measures of cell size and shape (Fig. 1e, see Methods). As expected from the rise in mean expression, *dig1 dig2* double mutants displayed less variability than wild-type in mating pathway outputs (Fig. 1c). The effect of deleting *DIG1* on noise is specific to outputs of the mating pathway, as the deletion of *DIG1* or *DIG2* did not affect the variability in three Ste12-independent reporters, *pPMP1-GFP, pYEF3-GFP* and *pAGP1-GFP* (Fig. 1c,d, Supplementary Information, Fig. S2). Furthermore, the changes in noise cannot merely be due to changes in the mean expression or growth rate since the analysis of several additional mutants illustrate that increased mean output and decreased growth rate do not result in increased noise (Supplementary Information, Fig. S3).

Both intrinsic and extrinsic noise increase in *dig1* cell populations

Gene expression noise can be decomposed into intrinsic and extrinsic components using a two-colour reporter gene system in which distinct fluorescent proteins are expressed from identical promoters in the same cell[15]. Intrinsic noise is defined as the uncorrelated cell-to-cell variation in levels of these two fluorescent proteins and is thought to reflect stochastic fluctuations in gene expression itself[16-19]. Extrinsic noise is defined as the correlated variation in the levels of the two proteins. Although extrinsic noise is thought to be impacted by cell-to-cell variability in the global cellular state, its origins and effectors are considerably less well-understood[9,11,14].

Using a two-colour assay with strains containing GFP and mCherry driven by *pAGA1* (Fig. 3a), we observed that both intrinsic and extrinsic noise increased in *dig1* cell populations as compared to wild-type and *dig2* cell populations. This result can be seen qualitatively by the reduced density of cells in the centre of the scatter plot of the data for the *dig1* mutant relative to wild-type and *dig2* (Fig. 3b), indicating an increased spread in fluorescence values. Quantitative calculations also reveal increases in the CV measurements (Fig. 3c, Supplementary Information, Fig. S4). The extrinsic noise (η_{ext}) was 22.8% ($P = 0.035$) greater in magnitude in *dig1* cells as compared to wild-type, while the intrinsic noise (η_{int}) was 14.9% ($P = 0.009$) higher (Fig. 3c). These patterns of increased intrinsic and extrinsic noise in *dig1* populations were independent of cell size and shape and were specific to Ste12-dependent outputs (Fig. 3d-f, Supplementary Information, Fig. S4d,e).

Dig1 prevents formation of subnuclear foci of Ste12-GFP molecules

The increased extrinsic noise in *dig1* cell populations could result from the breakdown of a mechanism in which Dig1 limits fluctuations in the levels of the transcription factor Ste12 through an autoregulatory feedback loop at the Ste12 promoter[20-22]. However, this was not the case since replacing the Ste12-dependent Ste12 promoter had no effect on noise (Fig. 4). This posed the possibility that the mechanism by which Dig1 acts on Ste12-dependent genes to limit extrinsic noise is beyond correlations in upstream factors. Extrinsic noise is typically measured by quantifying the correlated variability in the expression from two identical promoters, in this case *pAGA1*. However, more generally, correlated or extrinsic noise in *pAGA1* output would be expected to increase in *dig1* cells if Dig1 limited the correlated expression of all Ste12 outputs in the cell. One way for this to occur would be if Ste12 target genes co-localized in space in the absence of Dig1. If this were the case, the spatial

proximity of these genes could increase the dependence of the expression of one Ste12 target gene on the expression of another, perhaps due to increased local concentration of activators. For example, if Ste12 target genes co-localized in space, the induction of one gene could stimulate the induction of a neighbouring Ste12 target gene. Thus, it would be expected that the expression of such co-localized genes would be more correlated, in turn resulting in an increase in extrinsic noise. Given that Ste12 has many known interacting partners and exhibits self-cooperativity[5,6,23-27], Dig1 may function to shield protein-protein interaction domains on Ste12 that would otherwise cause Ste12 to homo-dimerize or bind to other proteins. Therefore, the loss of Dig1 might allow DNA-bound Ste12 proteins to enable long-range interchromosomal interactions between Ste12 target genes.

Consistent with this possibility, Ste12-GFP molecules localized to subnuclear foci in *dig1* cells (Fig. 5a, white arrowheads), while Ste12-GFP displayed granular nucleoplasmic staining in both wild-type and *dig2* cells (Fig. 5a). Approximately 65% of *dig1* cells showed one or more Ste12-GFP foci (Fig. 5b). These foci did not co-localize with the nucleolus (Supplementary Information, Fig. S5a) and focus formation could not explained by changes in total Ste12 protein levels since these levels were unaltered in *dig1* and *dig2* cells, as measured by quantitative immunoblotting (Supplementary Information, Fig. S5b). *dig1 dig2* double mutants also exhibited Ste12-GFP foci, but a slightly higher nucleoplasmic accumulation of Ste12-GFP protein precluded accurate assessment and quantification (Supplementary Information, Fig. S5c). Focus formation in *dig1* cells was specific to Ste12 as the transcription factor Reb1-GFP displayed nucleoplasmic staining in wild-type, *dig1* and *dig2* cells (Fig. 5a).

Focus-suppressing function of Dig1 is not controlled by MAPK signaling

In wild-type cells, stimulation with pheromone does not induce formation of Ste12-GFP foci (Fig. 5c), indicating that an increase in signalling and transcriptional output is not sufficient to induce their formation. While it has been suggested that mating signalling inactivates Dig1[5,6], we found that this protein remains physically associated with target genes (presumably via Ste12) in cells treated with pheromone (Fig. 5d). Thus, consistent with our finding that Ste12-GFP foci do not form in wild-type cells upon pheromone stimulation, not all activities of Dig1 are eliminated by signalling.

Increased long-range interactions between Ste12-target genes in *dig1* cells

Using a genome-wide adaptation of the single-locus iChIP technique[28], we examined interactions between the Ste12 target locus, *pFUS1*, and the rest of the genome in wild-type and *dig1* cells (see Methods). The locus efficiently immunoprecipitated as seen by the large peak centred on the *FUS1* promoter on the left arm of Chromosome III (Fig. 6a). No enrichment was observed at the *pFUS1* locus in the absence of LacI (Supplementary Information, Fig. S6). The 5% of genes (269 genes) whose promoters displayed the largest differences in ChIP-chip signals between *dig1* cells and wild-type were analyzed (Supplementary Information, Table S1). Remarkably, of the 203 gene regulators for which genome-wide localization data are available[21], only targets of Ste12 and Tec1 displayed a statistically significant increase in interactions with the *FUS1* locus in *dig1* cells (Fig. 6b, similar results obtained for 1%, 3% and 10% cutoffs). Moreover, these physical interactions

were dependent on the presence of Ste12 (Fig. 6c, Supplementary Information, Table S1). Tec1 and Ste12 are known to interact and are found at promoters of genes involved in both mating and filamentous growth22,27. Well-studied genes implicated in these processes were prominently featured among those that displayed increased physical interactions with the *FUS1* locus in *dig1* cells (Fig. 6d). We constructed promoter-YFP fusions for 11 of these Ste12-target genes and found that the mean expression increased for seven upon deletion of *DIG1* (Supplementary Information, Fig. S7a). Rigorous analysis of the changes in noise for these genes is complicated by the fact that the means increase significantly and the relationships between the means and CVs are unknown. However, we note that the removal of Dig1 induces a broadening of the output distributions that is highly reminiscent of trends seen with the *pFUS1-YFP* and *pAGA1-YFP* reporter stains (Supplementary Information, Fig. S7b).

Nonredundant roles for Dig1 in growth, mating, and gene induction kinetics

Under basal conditions, the mating pathway must appropriately balance the level of signalling to avoid cell cycle arrest and mating projection formation induced by pathway activation with a requirement for maintaining basal signalling to express key pathway components29. This balance might be expected to be disrupted in *dig1* cells, with repercussions for growth under basal conditions and mating in the presence of a pheromone signal. Therefore, cell-to-cell variability in outputs of the mating pathway could influence fitness. We found that *dig1* cells grow more poorly than wild-type or *dig2* cells and this defect is rescued by the deletion of *STE12* (Fig. 7a,b). Additionally, *dig1* cells display a kinetic defect in cell-cell fusion compared to wild-type and *dig2*, as measured quantitatively using a fluorescent-based assay in which the accumulation of double-positive fluorescent cells was scored (Fig. 7c-e, Supplementary Information, Fig. S8, see Methods). This defect is unlikely to be due to the slight increase in mean pathway output in *dig1* cells since previous studies found that even large increases in basal signalling does not reduce mating efficiency30. The defect in fusion between mating partners is mirrored by two quantitative changes in the induction of pheromone-inducible genes in *dig1* cells (Fig. 8a). First, *dig1* cells display a larger proportion of cells that do not induce *pAGA1-YFP* or *pFUS1YFP* reporter genes in response to pheromone treatment (Fig. 8b). Second, the population of *dig1* cells that does respond to pheromone displays a reduced dynamic range in the induction of pheromone inducible gene expression (Fig. 8c).

DISCUSSION

Recent work has shown that *DIG1* and *DIG2* were derived from a single parental gene that existed prior to the whole-genome duplication (WGD) that occurred in the ancestor of *S. cerevisiae* 100-200 million years ago31. Their continued presence in the genome suggests that their maintenance has an adaptive role. Indeed, previous work indicates that Dig1 and Dig2 inhibit Ste12 by interacting with distinct domains of the transcription factor, implying biochemical specialization 7,8. However, their genetic redundancy for inhibiting Ste12 was puzzling. Studies presented here revealed three functions of Dig1 that are not redundant with those of Dig2: 1) control of gene expression noise, 2) regulation of the intranuclear distribution of Ste12, and 3) the control of long-range interactions between Ste12-target

genes. We discuss below how these three functions may be related and the broader implications of these findings.

Dig1 is a well-studied regulatory protein that functions specifically in the pheromone response pathway and has only one reported biochemical function: to bind to a domain of Ste12 involved in protein-protein interactions5-8,32,33. The loss of Dig1 is, therefore, expected solely to unshield protein-protein interaction domains on the Ste12 transcription factor. Although indirect mechanisms are always difficult to rule out, we propose that this unshielding induces aggregation of Ste12 molecules and target genes, which results in increased cell-to-cell variability in the basal output of the pheromone response pathway. Dig2, which binds the distinct DNA-binding domain of Ste127, 8, does not share these functions. The aggregation of Ste12 molecules into one or two foci may create a domain within the nucleus where the transcription of Ste12-target genes can be activated. Our model suggests that the transcription of Ste12-target genes within the focus is more coordinated such that if one gene in the focus is transcribed, the others are, in turn, more likely to be expressed. Thus, such correlated expression within a single cell would be expected to yield increased correlated cell-to-cell variability in the transcriptional output of the pathway.

Transcriptional regulation that involves looping of DNA between distant sites via protein-protein interactions has been observed the *lac* operon34-38 and λ phage39,40. In the context of the results described here, it is notable that computational models of the *lac* system suggest that gene regulation by DNA looping can affect fluctuations in transcription41. These models predict that for transcriptional activators, DNA looping should increase noise in transcriptional outputs. Our model for the function of Dig1 is consistent with these theoretical predictions.

Recently, inter- and intrachromosomal interactions have been detected in other systems42-45. In erythroid cells, for example, Klf1-regulated genes, including *Hba* and *Hbb* globin genes, display long-range inter- and intrachromosomal interactions42. Although such interactions tend to correlate with transcriptional regulation and sites of active transcription, their precise functions remain a matter of considerable debate. Our observations suggest that while these long-range interactions could be important for gene expression, they may come at the cost of increased variability. This notion is in concordance with an emerging view that, in some cases, such gene interactions can be deleterious and even mutagenic46. It will be interesting to explore whether mechanisms of noise regulation are pervasive among regulatory circuits that involve long-range DNA interactions and the extent to which gene localization is balanced with a need for limiting noise.

While establishing the generality of the effect of aggregate formation on output variability will require further investigation, we note that subcellular protein and DNA aggregation is not uncommon in biology. DNA replication and gene activation can occur in "factories" located at the nuclear periphery47-51. Sites of DNA damage along with proteins that respond to DNA damage form nuclear foci in yeast52,53. Telomeres are also known to cluster in the nucleus54. Cytoplasmic P-bodies are foci of proteins involved in mRNA degradation and translational inhibition55-57. Given our data, these foci may serve, in some cases, to promote simultaneity in cellular transactions. The development of assays that can

distinguish between correlated and uncorrelated noise in these systems would allow the testing of such concepts.

Supplementary Material

Refer to Web version on PubMed Central for supplementary material.

Acknowledgments

Appendix

Methods

Strains

All yeast strains used are derived from BY4743, of the s288c background, and are described in Supplementary Information, Table S2. Yeast knockouts were generated by conventional lithium acetate and polyethylene glycerol procedures. YFP, eGFP (from pFA6a-EGFP-HIS3MX) and mCherry (from pFA6a-mCherry-HIS3MX or pFA6a-GFPtomCherry-URA3MX from J.S. Weissman) reporters for the mating pathway were constructed using methods as described[58], while *pPMP1*-fluorophore fusions were constructed using plasmids pFA6a-EGFP-HIS3MX6 and pFA6a-GFPtomCherry-URA3MX from J.S. Weissman.

Growth and fluorescence measurements by flow cytometry

Single fluorescent strains used: YM1968, YM2091, YM2100, YM2105, YM2109, YM2112, YM3550, YM3593, YM3594, YM3760, YM3762, YM3763, YM3764, YM3766, YM3767, YM3769, YM3770, YM3771, YM3772, YM3773, YM3776-YM3782 YM3804-YM3814. Dual fluorescent strains used: YM2636, YM2871, YM2876 and YM3132. Cells were grown in 1 mL cultures for 36 hr in 96-well deep pocket plates (Costar). OD_{600} measurements were taken and cultures were diluted to an $OD_{600} = 0.08$ and grown for 10 hr. A Becton Dickinson LSR-II flow cytometer was used, along with an autosampler device (HTS) controlled by custom software, to collect data over a sampling time of 7 sec[11]. YFP and GFP were excited at 488 nm and fluorescence was collected through a 505-nm long-pass filter and HQ530/30 and HQ515/20 band-pass filters (Chroma Technology), respectively. mCherry was excited at 532 nm and fluorescence collected through 600-nm long-pass filter and 610/20 band-pass filters (Chroma Technology).

Data analysis

All data analysis was done using custom MATLAB software. Raw cytometry data were filtered to eliminate errors due to uneven sampling time and negative fluorescence readings. Bulk calculations were done on these processed data. To control for cell aggregates, as well

as cell size and shape, forward and side scatter (FSC and SSC) data were expressed on orthogonal axes and subpopulations of cells were selected using circular gates of increasing radii centred on the median FSC and SSC values[11]. Nineteen circular bins were created with radii of 6000, 9000, 10^4, $2*10^4$, $3*10^4$,…,$17*10^4$ arbitrary units were used. Results are shown for data in bin 5, with a radius of $3*10^4$. Data were used if at least 5000 cells were in this bin, but on average between 20,000-40,000 cells had FSC and SSC values within this gate. The coefficient of variation (CV) was used as a measure of total noise, while intrinsic/uncorrelated and extrinsic/correlated noise were calculated as described[15] using GFP and mCherry dual-colour strains (Supplementary Information, Table S2). T-tests were used to calculate level of significance for increases in noise in the *dig1* mutant strains.

FACS sorting and expression dynamics

YM2105 (*pAGA1-YFP dig1*) were grown to mid-log phase. The fluorescence distribution was determined. A narrow gate cantered on the middle of this distribution was created and cells with expression levels within this gate were sorted using a Becton Dickinson FACSAria cell sorter. Cells were spun down, resuspended in YPAD and grown at 30 C. Aliquots were removed and the fluorescence distributions determined for 30,000 cells using a Becton Dickinson LSR-II flow cytometer. Data was analyzed as described above.

Microscopy

YM2910, YM3102, YM3103, YM3104, YM3722, YM3723, YM3724, YM3774 and YM3775 were grown overnight to saturation in YPAD. Cultures were diluted back to an OD_{600} of 0.1 in YPAD and grown for 4 hr. Microscopy was performed using a DeltaVision deconvolution microscope, which was outfitted with Olympus Plan Apo 60- and 100-X objectives. Z-stacks were taken with 0.3 μm steps. DeltaVision deconvolution software was used to deconvolve and analyze these images. For Ste12-GFP, a 1 s exposure was used and for Nup188-mCh, a 0.5 s exposure was used. For Reb1-GFP, a 1.0 s exposure was used. For the Ste12-GFP and Nop7-mCherry colocalization experiments, a 0.5 s exposure was used for the FITC channel and a 0.2 s exposure was used for the rhodamine channel.

Quantitative immunoblotting

YM1953, YM2101, YM2315, and YM2102 were grown to log phase in YPAD and 3 OD_{600} were collected by centrifugation and snap-freezing. Pellets were re-suspended in 100 μl 2X protein loading buffer and 1:100 Sigma phosphatase inhibitor cocktails 1 and 2 and 1:260 Sigma protease inhibitor cocktail. Samples were boiled for 2 min and 50 μl Zirconia/silica beads (Biospec Products) were added. Samples were then vortexed on a platform vortex for 2 min. Samples were again boiled for 2 min and centrifuged at 14,000 x g for 10 min to remove cell debris. The supernatants were pulled off, boiled for 3 min and resolved on a 10% SDS-PAGE gel. Proteins were then transferred to nitrocellulose and immunoblotting was performed as described in the Li-COR Odyssey manual using αSte12 (1:1000, a gift from Ira Herskowitz), αTubulin (1:3000, AbCam), αRabbit-IR$_{800}$ (1:1000) and αRat-IR$_{680}$ (1:1000).

Growth rate

YM1953, YM2101, YM2315, YM2643, YM2248, YM3776, YM3777 and YM3778 were grown to log phase overnight in YPAD. These cultures were then diluted back to an OD_{600} = 0.2 (YM1953, YM2101, YM2315 and YM2643) or OD_{600} = 0.05 (YM2248, YM3776, YM3777 and YM3778) at t=0 and OD_{600} measurements were taken every hour. To avoid cultures reaching saturation and entering stationary phase, cultures were diluted periodically. This dilution was accounted for in the subsequent OD_{600}calculations. OD_{600} measurements at later time points were normalized to the OD_{600} at time = 0 min. Best-fit lines were calculated using DeltaGraph 5 graphing software.

Flow cytometry-based cell-cell fusion assay

A *MAT**a*** strain (YM2901) containing at the *TRP1* locus a construct consisting of the N-terminus (AA 1-158) of *eGFP* fused to a leucine zipper dimerization domain59 was constructed. *MAT*α strains (YM2903, YM3085, YM3086 and YM3087) containing at the *LEU2* locus a construct consisting of the C-terminus (AA 159-240) of *eGFP* fused to a leucine zipper dimerization domain59 as well as an *mCherry* marker driven by *pTEF2* integrated at the *LYS1* locus were also constructed. See supplementary methods for experimental details.

Pheromone time-course assay

YM1968, YM2091, YM2100 and YM2105 were grown into log phase over night in YPAD. Cultures were diluted back to an OD_{600} = 0.4 and 50 nM α-Factor was added. 1 mL aliquots were removed at t = 0, 15, 30, 60, 90, 120, 150, 180 and 240 min, washed with water, resuspended in 1 mL TE pH = 8 and fluorescence distributions were measured by flow cytometry. Data were analyzed as described above.

ChIP

Dig1-GFP ChIP was performed as described60, 61 with strains YM1731 and YM3747 using an anti-GFP antibody from AbCam (Ab290). 5 μM α-Factor was added to log phase cultures for 1 hr.

Modified ChIP-chip method

An 11 kb construct consisting of 240 tandem arrays of Lac operators62 and an associated *HIS3MX* marker was inserted 331bp upstream of the *FUS1* ATG in strains containing a mCherry-LacI plasmid (BHM1336 adapted from pJH212, strains: YM3587, YM3588 and YM3687). Cultures were prepared for ChIP-chip by overnight growth to saturation in –Ura medium. Cultures were then diluted to an OD_{600} of 0.01 and grown for 4 hr in –Ura medium. These cells were again diluted to an OD_{600} of 0.01 in YPAD and collected 4 hr later. Chromatin immunoprecipitation was performed as described60,61. However, the protein crosslinker ethylene glycolbis (succinimidylsuccinate) (EGS) was added to a final concentration of 1.5 mM for 30 min before the addition of formaldehyde. Additionally, DNA was lightly sonicated in a Diagenode Bioruptor for 2×5 min on the low setting with 1 s on/ 0.5 s off pulses. To immunoprecipitate mCherry-LacI, a polyclonal anti-DsRed antibody from Clontech (catalogue number 632496) was used at a 1:100 dilution. Following ChIP,

strand displacement amplification and labelling were performed as described to generate DNA probes with incorporated aminoallyl-dUTP63. Probes representing mCherry-LacI immunoprecipitates and whole cell extracts were differentially labelled with Cy fluorescent dyes and hybridized on Agilent yeast whole-genome tiling microarrays (G4491A). Hybridization and array washing were performed as described by Agilent Technologies (Version 9.2). In addition, after the acetonitrile wash, slides were rinsed in Agilent Stabilization and Drying Solution (5185-5979). Microarrays were scanned at 5 μm resolution on a GenePix 4000B scanner (Molecular Devices) using GenePixPro 6.0 software. Microarray analysis was done using in-house software as described64. See supplementary methods for details of data analysis.

References

1. Marine JC, et al. Keeping p53 in check: essential and synergistic functions of Mdm2 and Mdm4. Cell Death Differ. 2006; 13:927–934. [PubMed: 16543935]

2. DeGregori J, Johnson DG. Distinct and Overlapping Roles for E2F Family Members in Transcription, Proliferation and Apoptosis. Curr Mol Med. 2006; 6:739–748. [PubMed: 17100600]

3. Moustakas A, Heldin CH. The regulation of TGFbeta signal transduction. Development. 2009; 136:3699–3714. [PubMed: 19855013]

4. Xu L. Regulation of Smad activities. Biochim Biophys Acta. 2006; 1759:503–513. [PubMed: 17182123]

5. Tedford K, Kim S, Sa D, Stevens K, Tyers M. Regulation of the mating pheromone and invasive growth responses in yeast by two MAP kinase substrates. Curr Biol. 1997; 7:228–238. [PubMed: 9094309]

6. Cook JG, Bardwell L, Kron SJ, Thorner J. Two novel targets of the MAP kinase Kss1 are negative regulators of invasive growth in the yeast Saccharomyces cerevisiae. Genes Dev. 1996; 10:2831–2848. [PubMed: 8918885]

7. Bardwell L, Cook JG, Zhu-Shimoni JX, Voora D, Thorner J. Differential regulation of transcription: repression by unactivated mitogen-activated protein kinase Kss1 requires the Dig1 and Dig2 proteins. Proc Natl Acad Sci U S A. 1998; 95:15400–15405. [PubMed: 9860980]

8. Olson KA, et al. Two regulators of Ste12p inhibit pheromone-responsive transcription by separate mechanisms. Mol Cell Biol. 2000; 20:4199–4209. [PubMed: 10825185]

9. Colman-Lerner A, et al. Regulated cell-to-cell variation in a cell-fate decision system. Nature. 2005; 437:699–706. [PubMed: 16170311]

10. Yu RC, et al. Negative feedback that improves information transmission in yeast signalling. Nature. 2008; 456:755–761. [PubMed: 19079053]

11. Newman JR, et al. Single-cell proteomic analysis of S. cerevisiae reveals the architecture of biological noise. Nature. 2006; 441:840–846. [PubMed: 16699522]

12. Cagatay T, Turcotte M, Elowitz MB, Garcia-Ojalvo J, Suel GM. Architecture-dependent noise discriminates functionally analogous differentiation circuits. Cell. 2009; 139:512–522. [PubMed: 19853288]

13. Bollenbach T, et al. Precision of the Dpp gradient. Development. 2008; 135:1137–1146. [PubMed: 18296653]

14. Volfson D, et al. Origins of extrinsic variability in eukaryotic gene expression. Nature. 2006; 439:861–864. [PubMed: 16372021]

15. Elowitz MB, Levine AJ, Siggia ED, Swain PS. Stochastic gene expression in a single cell. Science. 2002; 297:1183–1186. [PubMed: 12183631]

16. McAdams HH, Arkin A. Stochastic mechanisms in gene expression. Proc Natl Acad Sci U S A. 1997; 94:814–819. [PubMed: 9023339]

17. Becskei A, Kaufmann BB, van Oudenaarden A. Contributions of low molecule number and chromosomal positioning to stochastic gene expression. Nat Genet. 2005; 37:937–944. [PubMed: 16086016]

18. Raser JM, O'Shea EK. Control of stochasticity in eukaryotic gene expression. Science. 2004; 304:1811–1814. [PubMed: 15166317]

19. Blake WJ, M KA, Cantor CR, Collins JJ. Noise in eukaryotic gene expression. Nature. 2003; 422:633–637. [PubMed: 12687005]

20. Ren B, et al. Genome-wide location and function of DNA binding proteins. Science. 2000; 290:2306–2309. [PubMed: 11125145]

21. Harbison CT, et al. Transcriptional regulatory code of a eukaryotic genome. Nature. 2004; 431:99–104. [PubMed: 15343339]

22. Zeitlinger J, et al. Program-specific distribution of a transcription factor dependent on partner transcription factor and MAPK signaling. Cell. 2003; 113:395–404. [PubMed: 12732146]

23. Dolan JW, Fields S. Overproduction of the yeast STE12 protein leads to constitutive transcriptional induction. Genes Dev. 1990; 4:492–502. [PubMed: 2193847]

24. Yuan YL, Fields S. Properties of the DNA-binding domain of the Saccharomyces cerevisiae STE12 protein. Mol Cell Biol. 1991; 11:5910–5918. [PubMed: 1944269]

25. Baur M, Esch RK, Errede B. Cooperative binding interactions required for function of the Ty1 sterile responsive element. Mol Cell Biol. 1997; 17:4330–4337. [PubMed: 9234690]

26. Errede B, Ammerer G. STE12, a protein involved in cell-type-specific transcription and signal transduction in yeast, is part of protein-DNA complexes. Genes Dev. 1989; 3:1349–1361. [PubMed: 2558054]

27. Madhani HD, Fink GR. Combinatorial control required for the specificity of yeast MAPK signaling. Science. 1997; 275:1314–1317. [PubMed: 9036858]

28. Hoshino A, Fujii H. Insertional chromatin immunoprecipitation: a method for isolating specific genomic regions. J Biosci Bioeng. 2009; 108:446–449. [PubMed: 19804873]

29. Fields S, Chaleff DT, Sprague GF Jr. Yeast STE7, STE11, and STE12 genes are required for expression of cell-type-specific genes. Mol Cell Biol. 1988; 8:551–556. [PubMed: 3280969]

30. Stevenson BJ, Rhodes N, Errede B, Sprague GF Jr. Constitutive mutants of the protein kinase STE11 activate the yeast pheromone response pathway in the absence of the G protein. Genes Dev. 1992; 6:1293–1304. [PubMed: 1628832]

31. Gordon JL, Byrne KP, Wolfe KH. Additions, losses, and rearrangements on the evolutionary route from a reconstructed ancestor to the modern Saccharomyces cerevisiae genome. PLoS Genet. 2009; 5:e1000485. [PubMed: 19436716]

32. Pi H, Chien CT, Fields S. Transcriptional activation upon pheromone stimulation mediated by a small domain of Saccharomyces cerevisiae Ste12p. Mol Cell Biol. 1997; 17:6410–6418. [PubMed: 9343403]

33. Chou S, Lane S, Liu H. Regulation of mating and filamentation genes by two distinct Ste12 complexes in Saccharomyces cerevisiae. Mol Cell Biol. 2006; 26:4794–4805. [PubMed: 16782869]

34. Kramer H, et al. lac repressor forms loops with linear DNA carrying two suitably spaced lac operators. EMBO J. 1987; 6:1481–1491. [PubMed: 3301328]

35. Whitson PA, Hsieh WT, Wells RD, Matthews KS. Influence of supercoiling and sequence context on operator DNA binding with lac repressor. J Biol Chem. 1987; 262:14592–14599. [PubMed: 3667592]

36. Whitson PA, Hsieh WT, Wells RD, Matthews KS. Supercoiling facilitates lac operator-repressor-pseudooperator interactions. J Biol Chem. 1987; 262:4943–4946. [PubMed: 3549713]

37. Eismann E, von Wilcken-Bergmann B, Muller-Hill B. Specific destruction of the second lac operator decreases repression of the lac operon in Escherichia coli fivefold. J Mol Biol. 1987; 195:949–952. [PubMed: 3116268]

38. Mossing MC, Record MT Jr. Thermodynamic origins of specificity in the lac repressor-operator interaction. Adaptability in the recognition of mutant operator sites. J Mol Biol. 1985; 186:295–305. [PubMed: 4087296]

39. Dodd IB, Perkins AJ, Tsemitsidis D, Egan JB. Octamerization of lambda CI repressor is needed for effective repression of P(RM) and efficient switching from lysogeny. Genes Dev. 2001; 15:3013–3022. [PubMed: 11711436]

40. Revet B, von Wilcken-Bergmann B, Bessert H, Barker A, Muller-Hill B. Four dimers of lambda repressor bound to two suitably spaced pairs of lambda operators form octamers and DNA loops over large distances. Curr Biol. 1999; 9:151–154. [PubMed: 10021390]

41. Vilar JM, Leibler S. DNA looping and physical constraints on transcription regulation. J Mol Biol. 2003; 331:981–989. [PubMed: 12927535]

42. Schoenfelder S, et al. Preferential associations between co-regulated genes reveal a transcriptional interactome in erythroid cells. Nat Genet. 2009

43. Spilianakis CG, Lalioti MD, Town T, Lee GR, Flavell RA. Interchromosomal associations between alternatively expressed loci. Nature. 2005; 435:637–645. [PubMed: 15880101]

44. Zhao Z, et al. Circular chromosome conformation capture (4C) uncovers extensive networks of epigenetically regulated intra- and interchromosomal interactions. Nat Genet. 2006; 38:1341–1347. [PubMed: 17033624]

45. Apostolou E, Thanos D. Virus Infection Induces NF-kappaB-dependent interchromosomal associations mediating monoallelic IFN-beta gene expression. Cell. 2008; 134:85–96. [PubMed: 18614013]

46. Lin C, et al. Nuclear receptor-induced chromosomal proximity and DNA breaks underlie specific translocations in cancer. Cell. 2009; 139:1069–1083. [PubMed: 19962179]

47. Brickner JH, Walter P. Gene recruitment of the activated INO1 locus to the nuclear membrane. PLoS Biol. 2004; 2:e342. [PubMed: 15455074]

48. Kitamura E, Blow JJ, Tanaka TU. Live-cell imaging reveals replication of individual replicons in eukaryotic replication factories. Cell. 2006; 125:1297–1308. [PubMed: 16814716]

49. Meister P, Taddei A, Gasser SM. In and out of the replication factory. Cell. 2006; 125:1233–1235. [PubMed: 16814710]

50. Taddei A, et al. Nuclear pore association confers optimal expression levels for an inducible yeast gene. Nature. 2006; 441:774–778. [PubMed: 16760983]

51. Branco MR, Pombo A. Intermingling of chromosome territories in interphase suggests role in translocations and transcription-dependent associations. PLoS Biol. 2006; 4:e138. [PubMed: 16623600]

52. Lisby M, Mortensen UH, Rothstein R. Colocalization of multiple DNA double-strand breaks at a single Rad52 repair centre. Nat Cell Biol. 2003; 5:572–577. [PubMed: 12766777]

53. Bishop DK. RecA homologs Dmc1 and Rad51 interact to form multiple nuclear complexes prior to meiotic chromosome synapsis. Cell. 1994; 79:1081–1092. [PubMed: 7528104]

54. Cockell M, Gasser SM. Nuclear compartments and gene regulation. Curr Opin Genet Dev. 1999; 9:199–205. [PubMed: 10322139]

55. Parker R, Sheth U. P bodies and the control of mRNA translation and degradation. Mol Cell. 2007; 25:635–646. [PubMed: 17349952]

56. Sheth U, Parker R. Decapping and decay of messenger RNA occur in cytoplasmic processing bodies. Science. 2003; 300:805–808. [PubMed: 12730603]

57. Cougot N, Babajko S, Seraphin B. Cytoplasmic foci are sites of mRNA decay in human cells. J Cell Biol. 2004; 165:31–40. [PubMed: 15067023]

58. Storici F, Durham CL, Gordenin DA, Resnick MA. Chromosomal site-specific double-strand breaks are efficiently targeted for repair by oligonucleotides in yeast. Proc Natl Acad Sci U S A. 2003; 100:14994–14999. [PubMed: 14630945]

59. Magliery TJ, et al. Detecting protein-protein interactions with a green fluorescent protein fragment reassembly trap: scope and mechanism. J Am Chem Soc. 2005; 127:146–157. [PubMed: 15631464]

60. Meneghini MD, Wu M, Madhani HD. Conserved histone variant H2A.Z protects euchromatin from the ectopic spread of silent heterochromatin. Cell. 2003; 112:725–736. [PubMed: 12628191]

61. Raisner RM, et al. Histone variant H2A.Z marks the 5′ ends of both active and inactive genes in euchromatin. Cell. 2005; 123:233–248. [PubMed: 16239142]

62. Lau IF, et al. Spatial and temporal organization of replicating Escherichia coli chromosomes. Mol Microbiol. 2003; 49:731–743. [PubMed: 12864855]

63. Nobile CJ, et al. Biofilm matrix regulation by Candida albicans Zap1. PLoS Biol. 2009; 7:e1000133. [PubMed: 19529758]

64. Hartley PD, Madhani HD. Mechanisms that specify promoter nucleosome location and identity. Cell. 2009; 137:445–458. [PubMed: 19410542]
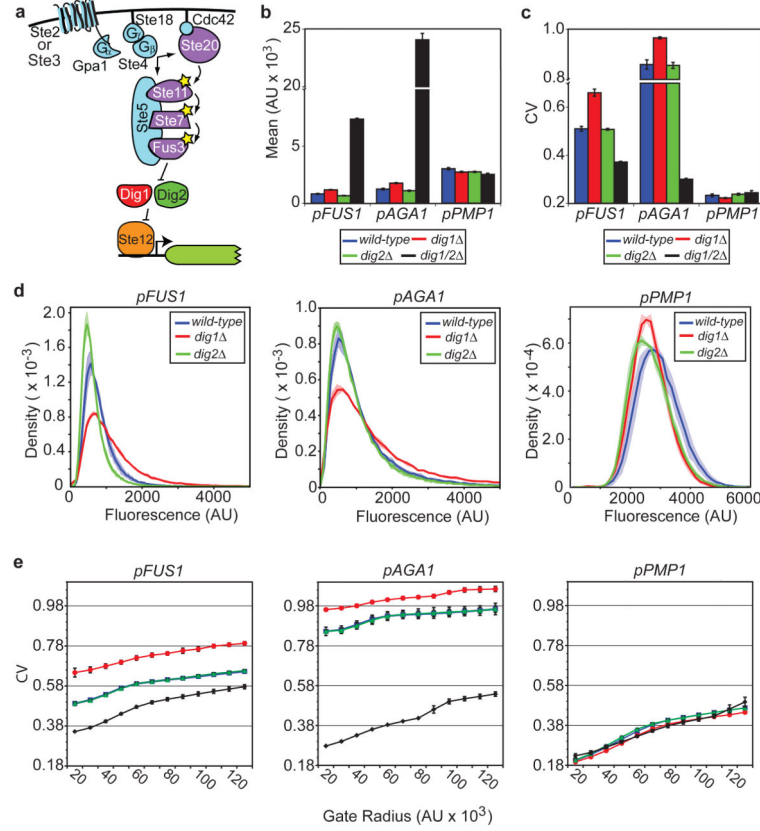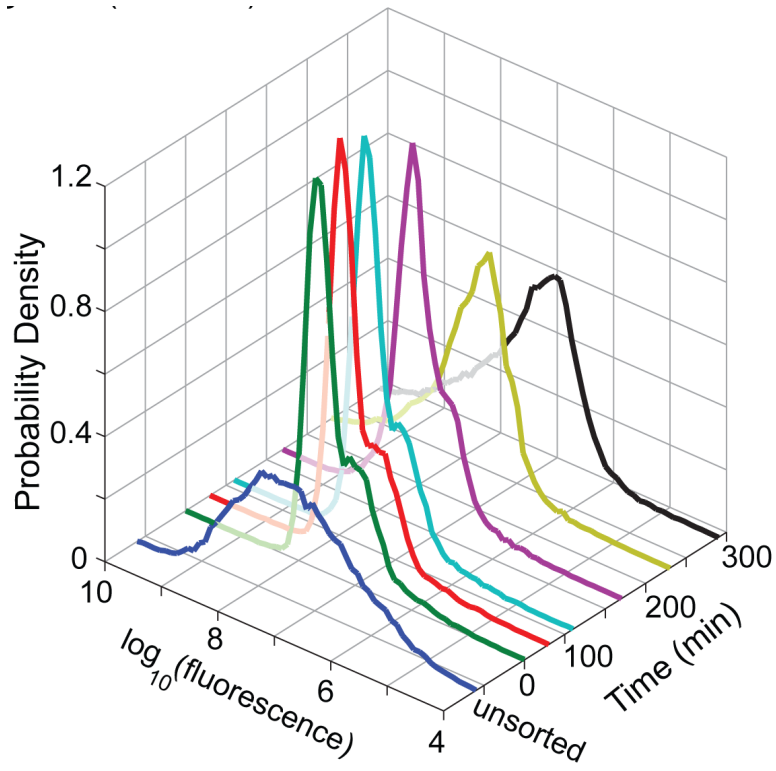
Figure 1.
dig1Δ, but not *dig2Δ*, cells display increased noise in yeast mating pathway outputs. **a.** Schematic of the yeast mating MAPK pathway. Note: for simplicity the Ste12-target gene is illustrated as having one Ste12-binding site. **b.** Mean output for *pFUS1-YFP, pAGA1-YFP*, and *pPMP1-GFP* in wild-type (blue), *dig1Δ* (red), *dig2Δ* (green), and *dig1Δ dig2Δ* (black) mutants in absence of α-Factor. Error bars indicate the standard deviation of three replicate experiments. The Y-axis is broken between 10,000 and 20,000 AU. **c.** Bar graphs illustrating the coefficient of variation (CV) for each strain as in **b**. The Y-axis is broken between 0.7 and 0.8. T-test was used to calculate $P = 0.0003$ for difference between *pAGA1-YFP* and *pAGA1-YFP dig1Δ* and $P = 0.0014$ for difference between *pFUS1-YFP* and *pFUS1-YFP dig1Δ*. **d.** Probability density functions (PDFs) of wild-type (blue) *dig1Δ (red)* and *dig2Δ* (green) for each reporter: *pFUS1-YFP* (left), *pAGA1-YFP* (middle) and *pPMP1-GFP* (right). Solid lines represent the average PDF for three replicates while the envelope indicates the standard deviation. (**b-d.** Data shown is for gate 5, see Methods.) **e.** CV vs. gate radius for *pFUS1-YFP* strains (left), *pAGA1-YFP* strains (middle) and *pPMP1-GFP* strains (right). **b-e.** See Methods for gate sizes and numbers of cells analyzed. Error bars represent the standard deviation of three replicate experiments.
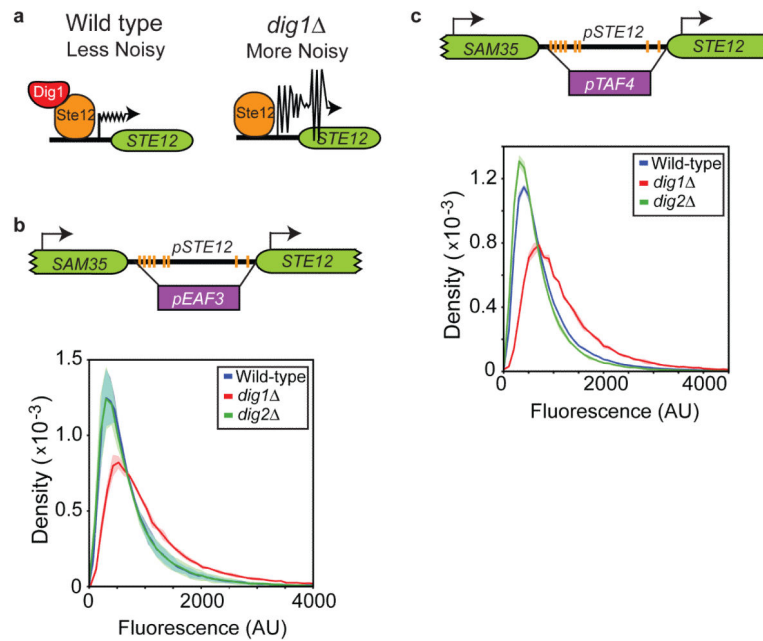
Figure 2.
Sorted *dig1* cells can regenerate the entire *pAGA1-YFP* output distribution. *dig1* cells expressing mean levels of *pAGA1-YFP* were sorted and re-grown over time. At t = 0, 60, 120, 180, 240 and 300 min, cells were removed and the fluorescence distribution was determined.
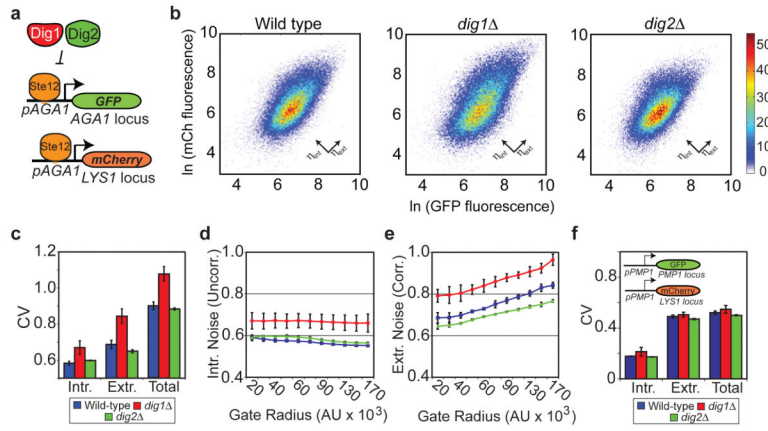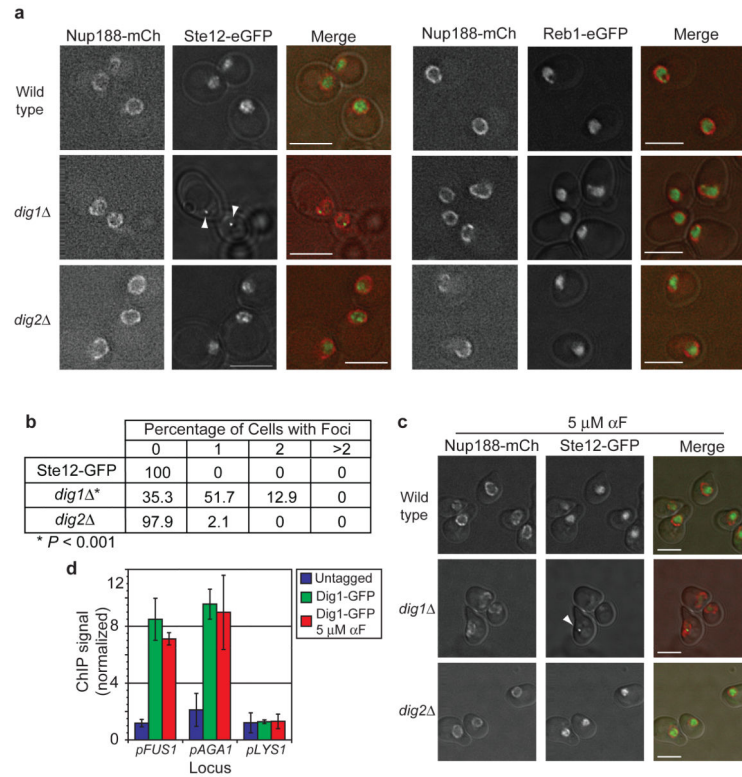
Figure 3.
Extrinsic and intrinsic noise in output of mating pathway increase in *dig1* cell populations. **A.** Schematic of two-colour experiment. *pAGA1-GFP* is in the endogenous *AGA1* locus, while *pAGA1-mCherry-AGA1 3'UTR* is inserted into the *LYS1* locus. **B.** Density plots of wild-type (left), *dig1* (middle) and *dig2* (right). **c.** Quantification of intrinsic, extrinsic and total noise of wild-type (blue), *dig1* (red), *dig2* (green) populations. Each value is the mean of three replicates and error bars indicate the standard deviation. T-test was used to calculate $P = 0.035$ for increase in intrinsic noise and $P = 0.009$ for increase in extrinsic noise in *dig1* mutant. Total noise was calculated as $\eta_{tot} = \sqrt{\eta_{ext}^2 + \eta_{int}^2}$. **d,e.** Plots of intrinsic (**d**) and extrinsic (**e**) noise vs. gate radius to control for cell size and shape. Error bars indicate the standard deviation of three replicates. **f.** Quantification of intrinsic, extrinsic and total noise in Ste12-independent reporter strain in which two fluorophores are driven by *pPMP1* (inset).
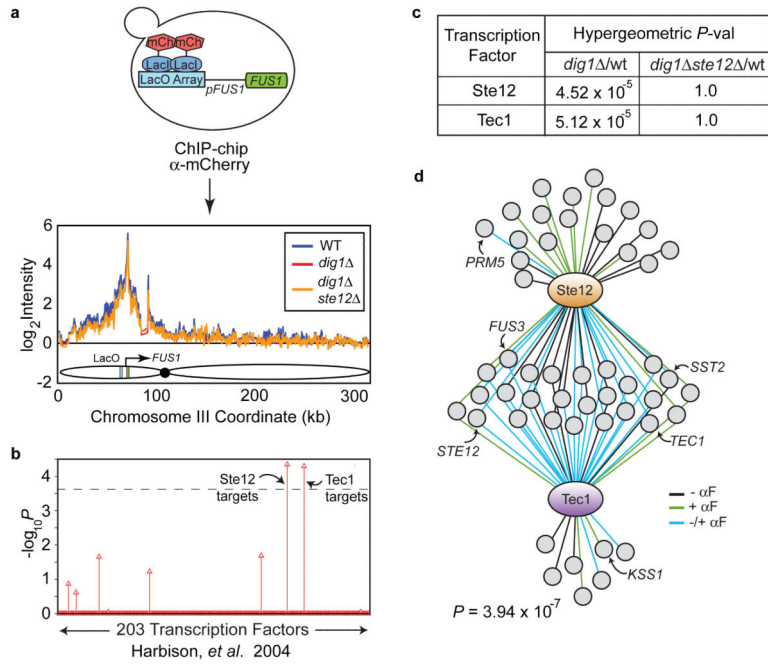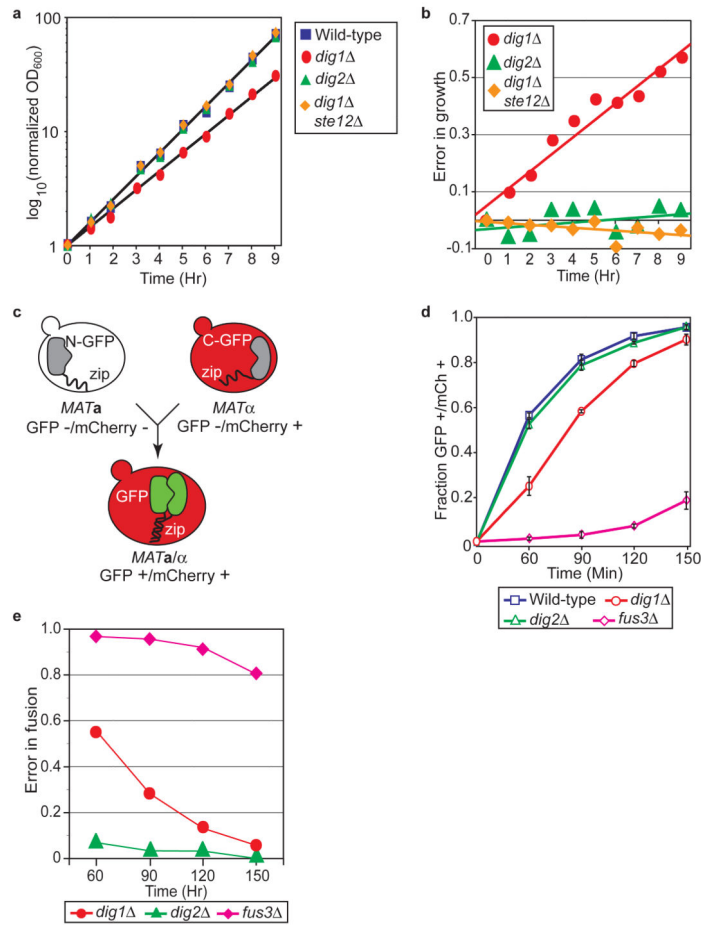
Figure 4.
Increased noise in mating pathway outputs in *dig1*Δ cells is not due to feedback at the *STE12* promoter. **a.** Model for the increased noise in the mating pathway in *dig1*Δ cells. **b.** *pSTE12* was replaced with the Ste12-independent promoter *pEAF3* (above). PDFs of *pAGA1-YFP* strains containing *pEAF3-STE12* (below). **c.** *pSTE12* was replaced with the Ste12-independent promoter *pTAF4* (above). PDFs of *pste12::pTAF4* strains (below). **b,c.** wild-type in blue, *dig1*Δ in red and *dig2*Δ in green. Solid line is the mean of three replicate experiments and the envelope reflects standard deviation of three replicates.
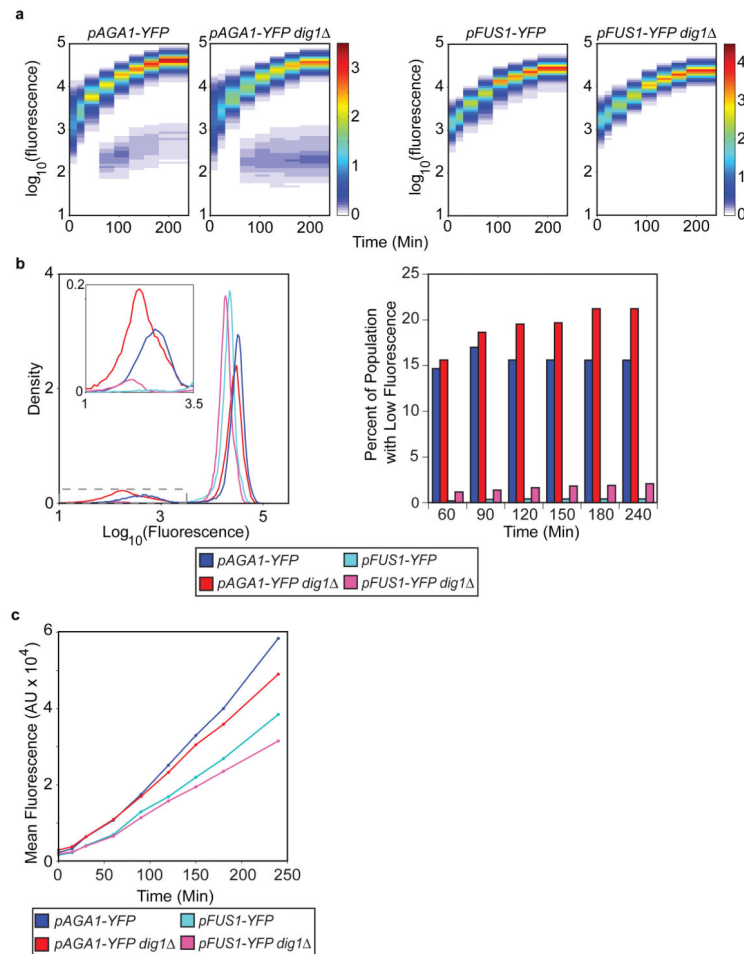
Figure 5.

Ste12-GFP forms nuclear foci in *dig1* cells. **a.** Fluorescence microscopy images of Ste12-GFP/Nup188-mCherry (left) and Reb1-GFP/Nup188-mCherry (right) from top to bottom: wild-type, *dig1*, and *dig2*. Ste12-GFP forms nuclear foci in *dig1* (see white arrow heads). **b.** Quantification of foci seen in (**a**) n = 100 (wt), n = 116 (*dig1*), n = 95 (*dig2*). Distributions of foci in all mutants were compared to wild-type by the Chi-square test and only the distribution of foci in *dig1* was statistically significant (*P* < 0.001). **c.** Ste12-GFP localization upon addition of 5 μm α-Factor for 1 hr. **d.** Normalized ChIP signal of Dig1-GFP at *AGA1, FUS1* and *LYS1* promoters in absence and presence of 5 μM pheromone. Scale bar for all images is 5 μm.

Figure 6.

ChIP-chip of Ste12-target locus reveals long-range interactions with other Ste12-target genes. **a.** Experimental set-up. LacI-mCherry was immunoprecipitated from cells and the *FUS1* locus (green), marked with an array of Lac operators (light blue), was efficiently pulled down (see peaks centred on Lac operators in graph below) in wild-type (blue), *dig1Δ* (red) *and dig1Δ ste12Δ* (orange) cells. The graph below illustrates the ChIP-chip signal along chromosome 3, where the array of Lac operators is inserted. See Methods for experimental details. **b**. Difference maps were calculated and genes were aligned by increasing median value of the region spanning −500bp to 0bp, with respect to the translation start site. The top 5% of differences (269 genes, Supplementary Information, Table S1) were analyzed for enrichment of target genes of 203 transcription factors21. The dashed line indicates the Bonferroni-corrected P value of 0.05. **c.** Bonferroni-corrected *P* values for enrichment of Ste12- and Tec1-target genes in the top 5% of genes with the greatest differences in *dig1Δ* vs. WT and *dig1Δ ste12Δ* vs. WT (Supplementary Information, Table S1). **d.** Ste12- and Tec1 target genes (in presence and absence of pheromone21) found in the list of 5% of genes with the largest differences in *dig1Δ* vs. WT datasets. *P* values calculated by hypergeometric testing.

Figure 7.

dig1 cells display defects in growth and cell-cell fusion. **a.** Log phase wild-type (blue squares), *dig1* (red circles), *dig2* (green triangles) and *dig1 ste12* (orange diamonds) cells were grown for 9 hrs and OD_{600} was measured every hour. **b**. Error in growth. OD_{600} of mutant (*dig1* in red, *dig2* in green and *dig1 ste12* in orange) was compared to that of wild type by calculating: $1 - [OD_{600}(\text{mutant})]/OD_{600}(\text{wild-type})]$. **c.** Schematic for FACS-based cell fusion assay. See Methods for details. **d.** Fraction of GFP+/mCherry+ cells over time for wild-type (blue), *dig1* (red), *dig2* (green) and *fus3* (pink). Samples were analyzed at 0, 60, 90, 120 and 150 min. Error bars indicate the standard deviation of three replicates. **e.** Cell-cell fusion error for mutants *dig1* in red, *dig2* in green and *fus3* in pink was calculated in the following manner: $1 - [(\text{fraction mutant fused})/(\text{fraction wild-type fused})]$.

Figure 8.
Time course of induction of *pAGA1-YFP* and *pFUS1-YFP* after treatment with pheromone.
a. Heat map of induction of *pAGA1-YFP* (left) and *pFUS1-YFP* (right) in wild-type and *dig1*Δ cells. Samples were analyzed at 0, 15, 30, 60, 90, 120, 150, 180 and 240 min. **b.** *left*: Probability density functions for 150 min time point of *pAGA1-YFP* (dark blue), *pAGA1-YFP dig1*Δ (dark red), *pFUS1-YFP* (light blue) and *pFUS1-YFP dig1*Δ (pink). The inset is a blow-up of the area marked by the grey-dashed line. *right*: The percentage of cells in the low fluorescence population versus time. **c.** Mean fluorescence of the transcriptionally induced populations in part **a** versus time. Transcriptionally induced and un-induced populations (see **a**) were separated and the means of the high expressing populations were calculated for each time point. The colours are as in part **b**. **a-c.** Data shown are from a single representative experiment, but results have been replicated in three separate experiments.